Note: This copy is for your personal non-commercial use only. To order presentation-ready copies for distribution to your colleagues or clients, contact us at *www.rsna.org/rsnarights.*

Prostate Cancer: Diagnostic Performance of Real-time Shear-Wave Elastography[1]

Jean-Michel Correas, MD, PhD
Anne-Marie Tissier, MD
Ahmed Khairoune, MD
Viorel Vassiliu, MD
Arnaud Méjean, MD, PhD
Olivier Hélénon, MD
Richard Memo, MD
Richard G. Barr, MD, PhD

Purpose: To prospectively evaluate the performance of real-time ultrasonographic (US) shear-wave elastography (SWE) in the diagnosis of peripheral zone prostate cancer in patients with high and/or increasing prostate-specific antigen levels and/or abnormal digital rectal examination results.

Materials and Methods: After signing an informed consent form, men referred for transrectal prostate biopsy were enrolled in this prospective HIPAA-compliant two-center study, which was conducted with institutional review board approval. Transrectal US SWE of the prostate was performed after a conventional transrectal US examination and immediately before US-guided 12-core sextant biopsy. For each sextant, the maximum SWE value was measured and matched to the pathologic results of that sextant biopsy. The diagnostic performance of SWE was assessed at both patient and sextant levels. The elasticity value maximizing the Youden index was used to derive sensitivity, specificity, positive predictive value (PPV), and negative predictive value (NPV).

Results: The elasticity values were matched to pathologic results for a total of 1040 peripheral zone sextants in 184 men. One hundred twenty-nine positive biopsy findings (size, ≥3 mm; Gleason score, ≥6) were identified in 68 patients. The sextant-level sensitivity, specificity, PPV, NPV, and area under the receiver operating characteristic curve for SWE with a cutoff of 35 kPa for differentiating benign from malignant lesions were 96% (95% confidence interval [CI]: 95%, 97%), 85% (95% CI: 83%, 87%), 48% (95% CI: 46%, 50%), 99% (95% CI: 98%, 100%), and 95% (95% CI: 93%, 97%), respectively.

Conclusion: Use of a 35-kPa threshold at SWE may provide additional information for the detection and biopsy guidance of prostate cancer, enabling a substantial reduction in the number of biopsies while ensuring that few peripheral zone adenocarcinomas are missed.

©RSNA, 2014

Online supplemental material is available for this article.

[1] From the Departments of Adult Radiology (J.M.C., A.M.T., A.K.) and Histopathology (V.V., O.H.), Necker University Hospital, Paris, France; Department of Urology, Hôpital Européen Georges Pompidou, Paris, France (A.M.); Department of Urology, Northeastern Ohio Medical University, Youngstown, Ohio (R.M.); and Radiology Consultants, 250 DeBartolo Pl, Youngstown, OH 44512 (R.G.B.). Received March 5, 2014; revision requested April 24; revision received July 25; accepted August 25; final version accepted August 28. Supported by SuperSonic Imagine, Aix-en-Provence, France. **Address correspondence to** R.G.B. (e-mail: *rgbarr@zoominternet.net*).

©RSNA, 2014

Prostate cancer is the most commonly diagnosed malignancy in men (excluding skin cancer), with an estimated 790 000 cases in 2012 and 241 740 new cases diagnosed every year in the United States (1). For more than 30 years, the screening standard for prostate abnormalities has been the combination of digital rectal examination and prostate-specific antigen (PSA) testing. An abnormal or increasing PSA level or an abnormal digital rectal examination result triggers a 12-core sextant biopsy guided with transrectal ultrasonography (US). However, there are two major drawbacks of systematic biopsy: *(a)* the substantial number of unnecessary biopsies in patients with no or indolent cancer (2) and *(b)* the high false-negative rate (3,4). Increasing the number of core biopsies (up to 40) improves prostate cancer detection and yields a better estimation of the tumor volume and Gleason score (5) but increases cost, morbidity, and the rate of overdiagnosis of microscopic tumor foci (6–9) without completely ruling out prostate cancer (10).

Multiparametric magnetic resonance (MR) imaging is an increasingly used modality for prostate tumor detection and staging (11–16), particularly in candidates for radical prostatectomy (17–22). However, its performance varies depending on which combination of positive features is selected for cancer diagnosis (23) and the size and aggressiveness of the prostate cancer (24). Although the sensitivity of multiparametric MR imaging is high, its specificity remains low (25), its cost is high, and it is not currently recommended as a first-line diagnostic tool for prostate cancer (1).

Conventional transrectal US has limited sensitivity and specificity ranging from 40% to 50% for cancer detection (26–28). Other transrectal US techniques, such as contrast material–enhanced US, are currently being evaluated (29,30).

Prostate cancer is often stiffer than normal prostate tissue (31). The use of prostate transrectal US static (or strain) elastography improves the detection of stiff prostatic tissues (32–35). However, this technique exhibits several limitations, including the lack of uniform compression over the entire gland, operator dependency, artifacts caused by slippage of the compression plane (36), and the lack of quantitative elasticity information. Another technique based on acoustic radiation force impulse (37) has been evaluated and has shown promising initial results; however, this technique is not commercially available. Recently, MR elastography has also proved capable of providing an elasticity image of the prostate. Although MR imaging shows promise, only a few clinical studies have been performed yet, and these were performed in a limited number of patients (38,39).

To overcome these limitations, shear-wave elastography (SWE) has been utilized (40–43). SWE allows local measurements of prostate tissue stiffness as quantitative elasticity values in kilopascals. In contrast to strain elastography, SWE requires no compression of the rectal wall. SWE has shown promising preliminary results in the detection and characterization of prostate cancers (42,44) in a limited number of patients. Our study aims at assessing SWE performance in a larger cohort of patients.

Seventy to eighty percent of prostate cancers arise in the peripheral zone (45), which is directly adjacent to the rectum wall and is easily accessible to transrectal US and transrectal US SWE. Indeed, the European Association of Urology recommends that the first series of transrectal US–guided systematic biopsies are performed posteriorly in the peripheral zone for prostate cancer detection (45).

The aim of this two-center study was to prospectively evaluate the performance of real-time SWE in the diagnosis of peripheral zone prostate cancer in patients with high and/or increasing PSA levels and/or abnormal digital rectal examination results.

Advances in Knowledge

- Shear-wave elastography (SWE) is a US technique that improves the detection of prostate cancer with a high sensitivity and high negative predictive value (96% and 99%, respectively).
- Prostate cancer stiffness increases with Gleason score, especially for elevated (≥7) Gleason scores (P = .01).

Implications for Patient Care

- The use of SWE could increase the positive biopsy rate from 12.4% (129 of 1040) for systematic biopsies to 47.5% (124 of 261) if an elasticity threshold of 35 kPa is used, yielding a potential reduction in the overall number of required prostate biopsy cores by eliminating biopsy of areas with normal elasticity, without a substantial decrease in cancer detection.
- SWE may decrease peripheral zone sextant biopsy sampling error (and therefore the high false-negative rate of this procedure) owing to its high negative predictive value (99%).

Published online before print
10.1148/radiol.14140567 **Content codes:** GU US

Radiology 2015; 275:280–289

Abbreviations:
AUC = area under the ROC curve
CI = confidence interval
NPV = negative predictive value
PPV = positive predictive value
PSA = prostate-specific antigen
ROC = receiver operating characteristic
ROI = region of interest
SWE = shear-wave elastography

Author contributions:
Guarantors of integrity of entire study, J.M.C., A.M., R.G.B.; study concepts/study design or data acquisition or data analysis/interpretation, all authors; manuscript drafting or manuscript revision for important intellectual content, all authors; manuscript final version approval, all authors; agrees to ensure any questions related to the work are appropriately resolved, all authors; literature research, J.M.C., A.K., A.M., R.G.B.; clinical studies, all authors; experimental studies, A.M.T., V.V., A.M., R.M., R.G.B.; statistical analysis, J.M.C., A.M.; and manuscript editing, J.M.C., A.K., A.M., O.H., R.M., R.G.B.

Conflicts of interest are listed at the end of this article.

Materials and Methods

Portions of this study (quantification with shear-wave imaging) were not approved by the U.S. Food and Drug Administration. The study was approved by each institution's local ethics committee or institutional review board. All patients gave written informed consent. Equipment loans were obtained from SuperSonic Imagine (Aix-en-Provence, France). The authors had complete control of all data and analysis of data.

From June 2010 through September 2012, all consecutive patients who met the inclusion criteria and who were scheduled for prostate biopsy were enrolled in this prospective Health Insurance Portability and Accountability Act–compliant study from two recruiting sites—one in the adult radiology department of Necker University Hospital (Paris, France) (center 1) and one in the radiology department of Northeastern Ohio Medical University (Youngstown, Ohio) (center 2). Inclusion criteria were an elevated (>4.0) or increasing PSA (increase of more than half a point in a year) and/or an abnormal digital rectal examination result. Prostate biopsy was performed immediately after real-time SWE was performed by using the Aixplorer US diagnostic imaging system (SuperSonic Imagine) and an SE12–3 endocavity transrectal high-frequency (8-MHz) probe. Two physicians (one at each center) (J.M.C. and R.G.B., each with more than 20 years of experience in transrectal US and more than 2 years of experience in SWE prostate imaging) independently performed the measurements.

Transrectal US and SWE

Prostate SWE acquisitions were performed after an evaluation of the prostate with B-mode imaging in patients lying in the left lateral position to assess the size of the prostate and to guide systematic sextant biopsies within the prostate. The SWE mode was activated, and the entire gland was scanned in the transverse plane. SWE acquisitions were performed by avoiding pressure on the prostate applied with the transducer. Settings were adjusted to maximize penetration and to enable visualization of peripheral zone stiffness with a maximum elasticity scale of 70 kPa. SWE acquisition included the following steps: The elastographic box was enlarged to the maximum to cover half of the gland in a transverse plane, and each side of the peripheral zone of the prostate was scanned separately from base to apex by using a very slow movement that allowed stabilization of the signals. The two digital cine loops were stored to allow further stiffness measurements. Each digital cine loop was reviewed at the end of the SWE acquisition, and systematic stiffness measurement was performed at the maximum stiffness site within each peripheral zone sextant (two measurements per sextant placed in the stiffest part of the lateral and medial subregions of the sextant) by using a region of interest (ROI) (Fig 1). The ROI used for all measurements was round, and its diameter was adapted to enclose the areas of higher stiffness ranging from 3 to 7 mm (median, 5 mm). The same ROI size was used for suspicious- and for normal-appearing sextants. The ROI was placed on the peripheral zone on the basis of the B-mode image, on which the peripheral zone could be clearly identified (Fig 2).

Figure 1

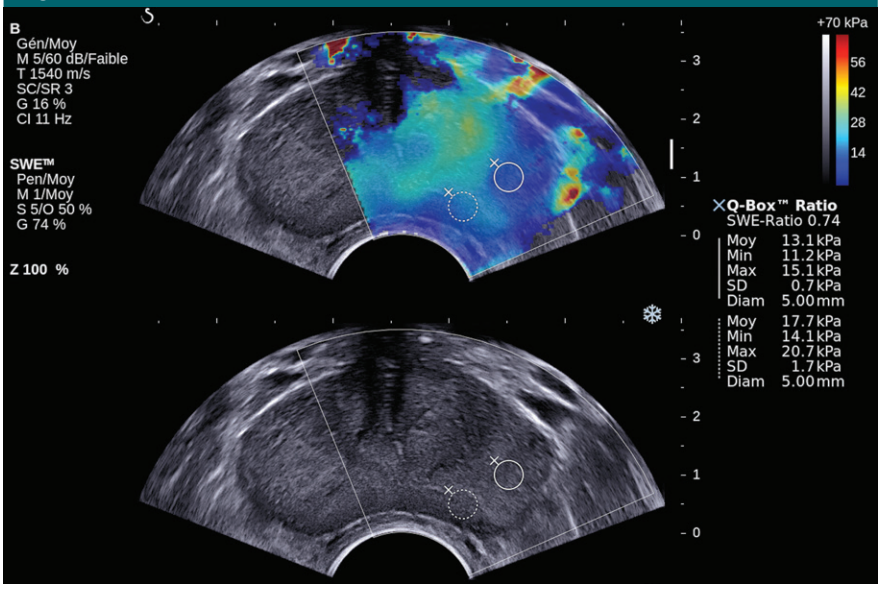

Figure 1: SWE prostate measurements in 58-year-old man with a PSA level of 4.6 ng/mL. The top image shows the color-coded SWE in the color box, while the bottom image shows the same plane with only B-mode information. SWE mean elasticity values were measured by placing two round ROIs in the paramedian and lateral sextants. Note the homogeneous pattern of the peripheral zone. Biopsies did not reveal any cancer, and elasticities throughout the prostate were low.

Biopsy and Pathologic Examination

After the SWE acquisitions, US-guided prostate biopsies were performed by one of two physicians (A.K., a uroradiologist, and R.M., a urologist, each with at least 20 years of experience in performing transrectal US prostate biopsies) using a biopsy guide attached to the US probe. These two physicians were blinded to the results of the SWE study. Systematic biopsies were performed with US guidance by using a disposable 18-gauge prostate needle (Programmable Automatic Biopsy System Achieve, CareFusion, San Diego, Calif [center 1]; or Tru-Cut needle, Bard, Covington, Ga [center 2]). The systematic biopsy protocol included 12 peripheral posterior biopsies, with paramedian and lateral cores for each sextant, unless there was a contraindication to biopsy because of treatment

Figure 2

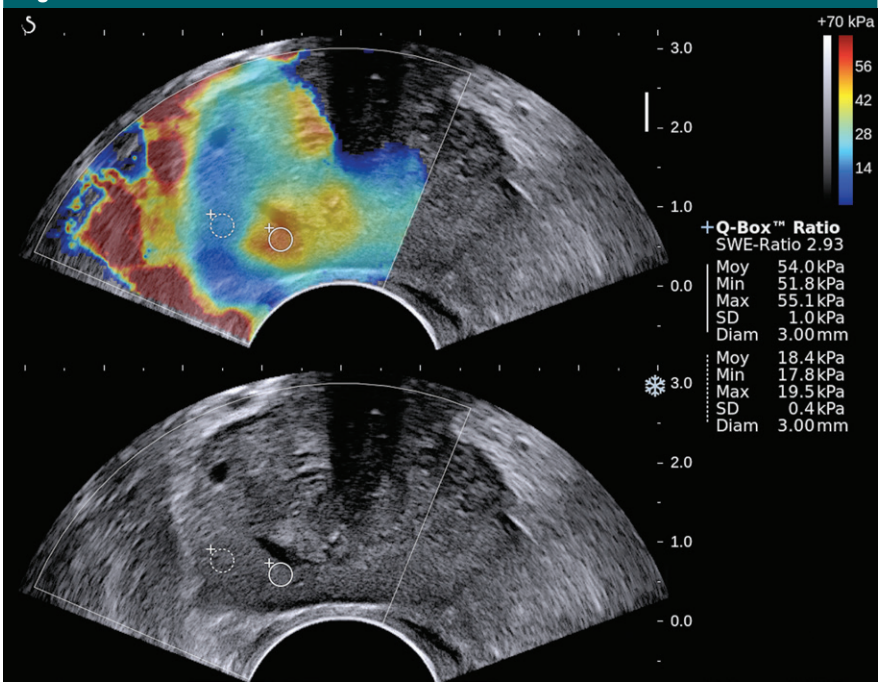

Figure 2: SWE prostate measurements in 57-year-old man with a PSA level of 6.62 ng/mL. The top image shows an orange-coded stiff area (solid-line ROI; mean elasticity, 54 kPa) incidentally discovered in the left base paramedian peripheral zone with no abnormal features at B-mode US (bottom image). Another ROI (dashed line; mean elasticity, 18.4 kPa) was located in the lateral peripheral zone of the same sextant. The biopsy performed in the stiffest area revealed an 11-mm Gleason 7 adenocarcinoma.

with platelet inhibitors or warfarin. In this case, a smaller number of biopsies were performed.

All specimens were analyzed by a single pathologist at each site (V.V. at center 1). Both pathologists had more than 15 years of experience in the evaluation of prostate core biopsy samples. The pathologist was blinded to the imaging results but not to the patient's clinical and biochemical data. The Gleason score and presence of prostatic intraepithelial neoplasia were determined for each specimen. The length of each biopsy specimen (in millimeters) was recorded, as well as the length of adenocarcinomatous tissue, if found, in the biopsy core. A biopsy was considered to have positive results (indicating malignancy) when the Gleason score was 6 or higher and the size of the adenocarcinomatous tissue within the biopsy core was 3 mm or larger. These criteria are commonly used to define clinically important prostate cancers; however, they are often debated as well (46).

Data Analysis

Data analysis was performed at the level of the prostate sextant and at the level of the patient. For each prostate sextant, the highest stiffness value between the paramedian and lateral measurements was used for statistical analysis. For the two systematic biopsies performed in the same sextant, prostate cancer was considered to be present if at least one of the two cores contained an adenocarcinoma, as defined according to the criteria described above. If the two cores in the same sextant were positive, the core used for Gleason score analysis and cancer tissue length was the one with the highest Gleason score. The biopsy results were grouped by sextant (maximum size and Gleason score) and were correlated with the stiffest area (in kilopascals) in the corresponding sextant.

For patient-level analysis, a patient was considered to have SWE-positive results if at least one sextant had an elasticity value higher than the cutoff value; otherwise, the patient was considered to have SWE-negative results. A patient was considered to have prostate cancer if at least one of the 12 systematic biopsy cores was positive (according to the criteria for prostate cancer defined above); otherwise, the patient was considered to be cancer free.

Statistical Analysis

Statistical analysis was performed by using R software *(http://cran.r-project.org/)*. The relationship between elasticity and each variable was assessed by using the Spearman rank correlation coefficient. Elasticity values of malignant and benign regions were compared by using a paired Student t test. $P < .05$ was considered to indicate a statistically significant difference. In assessing diagnostic accuracy, it is often essential to determine a test's ability to both detect and correctly locate multiple abnormalities per patient. The statistical method for clustered data to assess the test's accuracy described by Obuchowski et al (47,48) was used for patient-based analysis (assuming correlation among sextants in the same patients). A sextant-based (or ROI-based) conventional analysis was performed assuming no correlation among sextants from the same patient. Receiver operating characteristic (ROC) curves were plotted for elasticity values at sextant and patient levels, and areas under the ROC curve (AUCs) were calculated with 95% confidence intervals (CIs). Optimal elasticity cutoff values were determined by using the maximum Youden index (sensitivity + specificity − 1), assuming sensitivity and specificity were equally important. The sensitivity, specificity, positive predictive value (PPV), and negative predictive value (NPV) were then derived with corresponding 95% CIs for both sextant- and patient-based analyses. For patient-level analysis, the true-positive rate characterized the ability of SWE to reveal at least one malignant lesion in patients with cancer, and the false-positive rate described the frequency with which the test incorrectly revealed at least one abnormality in patients without an abnormality. The patient-level

Table 1

Demographic Data in Patient Population

Characteristic	Overall Population	Population at Center 1	Population at Center 2	*P* Value
No. of patients	184	106	78	.60
No. of patients with cancer	68 (37.0)	49 (46.2)	19 (24)	
Age (y)*	65.1 ± 7.6 (51–86)	65.8± 7.6 (51–86)	64.2 ± 7.4 (46–79)	.15
PSA (ng/mL)*	7.4 ± 6.6 (0.2–60)	9.1 ± 7.3 (0.4–60)	4.7 ± 3.7 (0.2–18.6)	<.001
Prostate volume (mL)*	52.0 ± 26.4 (12.9–159)	54.9 ± 24.1 (15–125)	48.0 ± 29.1 (12.9–159)	.09
No. of biopsies	1040	568	472	
No. of positive biopsies	129	86	43	
No. of negative biopsies	911	482	429	
Positive biopsy rate (%)	12.4	15.1	9.1	
No. of Gleason 6 biopsies	34 (26.4)	15 (17.4)	19 (44.2)	
No. of Gleason 7 biopsies	72 (55.8)	59 (68.6)	13 (30.2)	
No. of Gleason 8 biopsies	11 (8.5)	6 (7.0)	5 (11.6)	
No. of Gleason 9 biopsies	12 (9.3)	6 (7.0)	6 (14.0)	

Note.—Unless otherwise specified, data are numbers of patients or biopsies, with percentages in parentheses. Sextants with Gleason scores of 6–9 were considered to contain malignancy.

* Data are means ± standard deviations, with ranges in parentheses.

ROC areas were derived by plotting the patient-based false-positive rate versus the patient-based true-positive rate and were interpreted as the probability that SWE correctly helps distinguish between a patient with at least one malignant lesion and a patient with no cancer.

The correlation between Gleason score and adenocarcinoma stiffness was calculated by using Spearman rank correlation; elasticity value box-and-whisker plots were computed for each Gleason score. To take into account the spectrum effect and to prevent multiple-testing risks, a method for estimating the accuracy of a diagnostic test when the reference standard is not binary that was described by Obuchowski (49) was used. This method provides a multinomial version of the AUC. Pairwise AUC*st* values provide estimations of the diagnostic test's AUC for differentiating between categories *s* and *t*. In our study, five categories corresponded to the reference standard outcome (histologic Gleason scores); category 1 indicated benign tissue, and categories 2, 3, 4, and 5 indicated Gleason scores of 6, 7, 8, and 9, respectively. The measure, called the Obuchowski measure (*w*AUC), is a weighted average of the $n(n-1)/2$ different AUC*st* values corresponding to all pairwise comparisons between two of the *n* categories. Each pairwise comparison between stages was weighted to take into account the distance between grades (Gleason scores).

To determine the ability of SWE to reveal small prostate cancers, an analysis was performed that involved varying the size criterion used to define a positive biopsy core (the minimal size of the adenocarcinoma) from 2 to 12 mm.

Results

A total of 184 patients were enrolled in the study (Table 1). Of the 1104 sextants (six sextants per patient), 64 sextants (5.8%) had missing data. The reasons for the missing data were as follows: lack of SWE information because of SWE penetration issues (21 sextants [1.9%]), technical issues with SWE (33 sextants [3.0%]), and lack of pathologic results because of a limited number of biopsies performed in patients receiving platelet inhibitors or warfarin (10 sextants [0.9%]). A mean of 11.89 biopsies was performed per patient, with a range of six to 12 biopsies. Therefore, elasticity values from 1040 sextants were matched with the pathologic biopsy results. The positive biopsy rate was 12.4% (129 of 1040). Center 1 had a higher positive biopsy rate, which was probably related to higher PSA levels in its patient population. Prostate cancer grades were mainly Gleason 6 and 7 (106 [82.2%] of 129 cancers).

Sextant-level Results

A maximum Youden index of 81% (95% CI: 78%, 84%) was found, and use of a cutoff value of 35 kPa for SWE in differentiating benign from malignant sextants yielded an AUC of 95% (95% CI: 93%, 97%) (Table 2, Fig 3) and a *w*AUC of 96% (95% CI: 94%, 98%). Prostate cancer elasticity values ranged from 10 to 267 kPa, with a median and an interquartile range of 53 and 43 kPa, respectively. Benign sextants had Young moduli that ranged from 8 to 218 kPa, with a median and an interquartile range of 21 and 12 kPa, respectively ($P < .001$) (Fig 4).

In Table 3, AUC*st* estimation revealed significant differences between sextants in all Gleason categories and sextants of benign tissue, with all AUC*st* values being greater than 85% (95% CI: 79%, 91%), while the Gleason 6 category was less differentiated from Gleason 7 and 8 categories (AUC*st* = 46% [95% CI: 78%, 84%] and AUC*st* = 68% [95% CI: 48%, 88%], respectively) (Fig 5). There was also a less marked difference between Gleason 7 and 8 categories (AUC*st* = 70% [95%

Table 2

Sextant- and Patient-level Performance of SWE

Performance Level	Maximum Youden Index (%)	SWE Cutoff (kPa)	Sensitivity (%)	Specificity (%)	PPV (%)	NPV (%)	AUC (%)
Per sextant	81 (78, 84)	35 (35, 35)	96 (95, 97) [124/129]	85 (83, 87) [774/911]	48 (46, 50) [124/261]	99 (98, 100) [774/799]	95 (93, 97)
Per patient	56 (45, 65)	38 (37, 38)	93 (89, 96) [63/68]	63 (56, 70) [73/116]	59 (52, 66) [103/106]	94 (88, 100) [73/78]	80 (72, 87)

Note.—Data in parentheses are 95% CIs; data in square brackets are those used to calculate the percentages.

CI: 54%, 96%]). Gleason 9 sextants were very differentiated from all other Gleason score categories (AUC*st* ≥ 83%). Elasticity of malignant sextants as a function of prostate cancer size (Figs 6, E1 [online]) for each Gleason score had a Spearman rank correlation coefficient of 0.282 ($P < .001$). A statistically significant difference in stiffness was found between Gleason 6, 7, and 8 categories and the Gleason 9 category ($P < .0000001$), as well as between Gleason 6 and 7 and Gleason 8 and 9 categories ($P = .001$), but this difference was less marked between the Gleason 6 category and Gleason 7, 8, and 9 categories ($P = .01$).

Sextant-based ROC curves for SWE were also plotted, and the sensitivity, specificity, PPV, NPV, and AUC were calculated for different minimal prostate cancer sizes ranging from 2 to 12 mm for a fixed elasticity cutoff of 35 kPa (Figs 7, E2 [online]). The elasticity AUC was 95% (95% CI: 93%, 97%) for a minimal prostate cancer size of 3 mm, while the NPV was 99% (95% CI: 98%, 100%), sensitivity remained above 95% (ranging from 95% to 97%) (95% CI: 95%, 97%), and specificity stayed above 80% (ranging from 80% to 85%) (95% CI: 83%, 87%). The PPV decreased from 48% to 25% with increasing minimal size. The accuracy also decreased with increasing cutoff size, from 55% (for a 2-mm minimal prostate cancer size) to 30% (for a 12-mm minimal size). This raises the issue that when the size cutoff was increased, smaller cancers were considered false-positive findings in the analysis. The optimal Youden index of 81% (95% CI: 78%, 84%) was found for a minimal prostate cancer size of 3 mm.

The performance of SWE was also assessed for different prostate cancer minimal sizes (Figs 7, E2 [online]). The Youden index, sensitivity, specificity, PPV, NPV, AUC, and ROC curves were computed for several prostate cancer minimal sizes ranging from 2 to 12 mm (Figs 7, E2 [online]). Sensitivity slightly increased for prostate cancers larger than 8 mm (sensitivity, 98%); however, PPV drastically decreased to less than 25% (because small cancers are stiff but are not considered malignant).

Figure 3

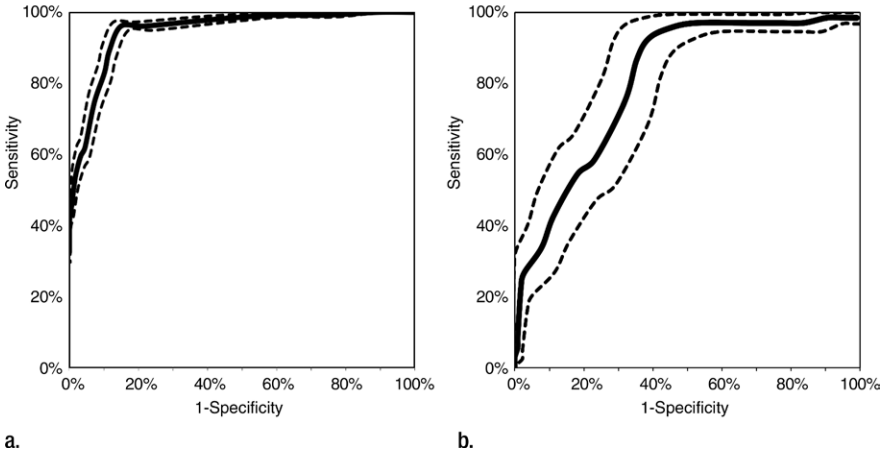

Figure 3: **(a)** ROC curve for sextant SWE shows an AUC of 95%. **(b)** ROC curve for patient SWE shows an AUC of 80%. Dashed lines = 95% CIs for the ROC curves.

Patient-level Results

The maximum Youden index to differentiate patients with from those without cancer was 38 kPa. The SWE technique exhibited an AUC of 80% (95% CI: 72%, 87%) (Table 2, Fig 3).

Discussion

By maximizing sensitivity and specificity, the highest Youden index allowed us to determine a cutoff of 35 kPa. At the sextant level, a 35-kPa SWE cutoff value yielded 96% sensitivity (124 of 129 [95% CI: 95%, 97%]) for prostate cancer detection, as well as a high NPV of 99% (774 of 779 [95% CI: 98%, 100%]), with an AUC of 95% (95% CI: 93%, 97%).

For a cutoff of 30 kPa, the PPV decreased to 35% (95% CI: 33%, 37%), while for a threshold of 40 kPa, the sensitivity decreased to 82% (95% CI: 80%, 84%).

At present, the success rate of systematic prostate biopsy ranges from 25% to 30%, while its false-negative rate varies from 17% to 21% in patients with a negative first series of biopsies (3,4). In our study, there was a 12.4% (129 of 1040) positive rate for systematic biopsies at the sextant level and a 37.0% (68 of 184) positive rate at the patient level. If SWE had been used with an elasticity threshold of 35 kPa, the number of systematic biopsies could have been reduced by 74.4% (774 of

Figure 4

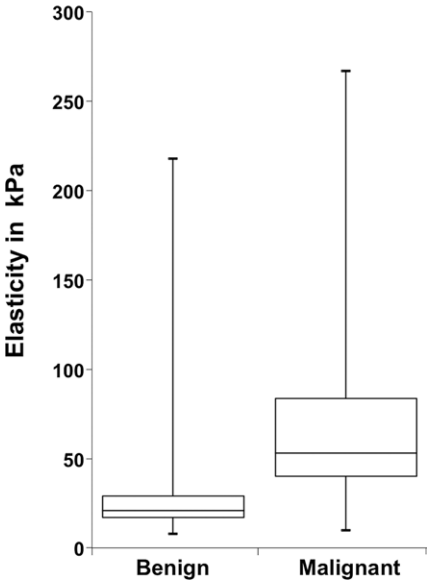

Figure 4: Box-and-whisker plot shows elasticity values for benign and malignant prostate sextants. Boundaries of boxes = 25th and 75th percentiles ($P < .001$).

Figure 5

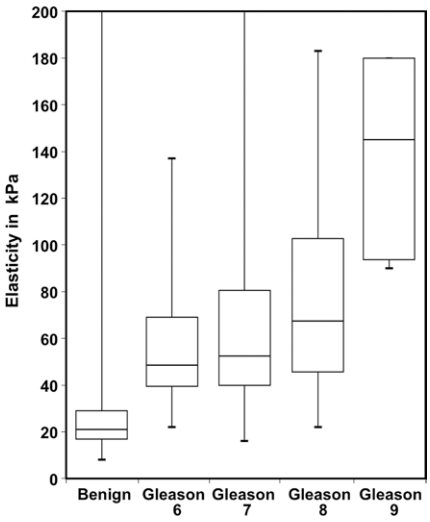

Figure 5: Box-and-whisker plot shows elasticity values for benign and malignant sextants with Gleason scores of 6, 7, 8, and 9. Boundaries of boxes = 25th and 75th percentiles.

Figure 6

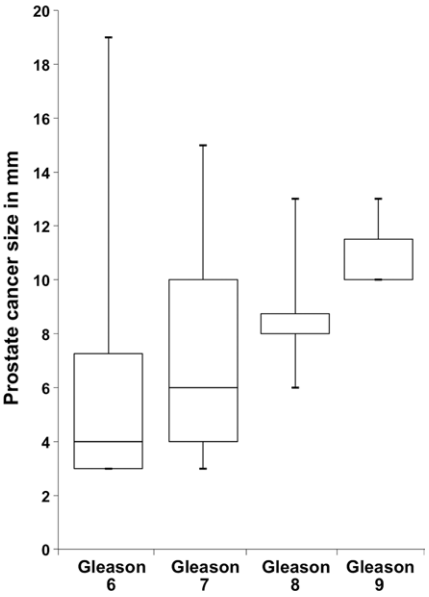

Figure 6: Box-and-whisker plot shows adenocarcinoma size for different Gleason scores. Boundaries of boxes = 25th and 75th percentiles.

the 1040 systematic biopsies), yielding a positive biopsy rate of 47.5% (124 of 261). The high NPV of SWE may in the future be used to reduce the number of systematic biopsies and, moreover, to reduce the need for invasive procedures such as systematic biopsies. Indeed, the patient-level analysis showed that 39.7% of the patients (73 of 184) enrolled in this study could have avoided transrectal US systematic biopsy if SWE had been used to select patients for this procedure. The patient-level analysis also showed a high NPV of 94% (73 of 78) and a high sensitivity of 93% (63 of 68) for SWE.

These results, in terms of sensitivity, specificity, and NPV, are in agreement with those reported in previous preliminary studies by Barr (50) and Ahmad et al (44), which exhibited sensitivities ranging from 90% to 96%, specificities ranging from 88% to 99%, and NPVs ranging from 81% to 99%. However, the PPV was higher for Barr at 69% and for Ahmad et al at 98% than for our study (at 48%). This difference could be explained by a difference in patient populations: Mean PSA levels were 5 ug/L for the Barr study, greater than 20 ug/L for the Ahmad et al study, and 7.1 ug/L in our population. All studies reported a significantly higher stiffness for prostate cancer than for benign tissues ($P < .05$ for all), with a trend toward differences in stiffness between different Gleason scores for Ahmad et al (44).

From the prostate cancer analysis, it can be inferred that SWE can efficiently reveal prostate cancers of 3 mm or larger (sensitivity, >95%). The ability to reveal cancers and guide biopsies in areas suspicious for cancer will also help improve prostate cancer detection rates.

In our study, two statistical analyses were performed to assess SWE performance in the detection and localization of malignant prostatic lesions: a patient-based approach and a ROI-based or sextant-based approach. The patient-based approach considers the potential for multiple findings in the same patient and their localization. For example, a patient with a single false-positive lesion is treated in the same manner as a patient with multiple false-positive lesions. This causes both the numerator and denominator of the false-positive rate to be different from those in the sextant evaluation. Also, patients can have both true-positive and false-positive findings. This explains the lower observed diagnostic performance of SWE in the per-patient analysis. The ROI-based 95% CIs were also smaller than those for the patient-based estimates in almost every case. The sextant-based approach will, in general, be more powerful than the patient-based approach, as clinical treatment can be tailored to each sextant. A negative SWE examination in a sextant may decrease the number of biopsies required.

Our study had several limitations. It used transrectal US–guided systematic biopsy results as the reference standard for prostate cancer detection. Even though this technique is the recommended diagnostic method in most patients suspected of having prostate cancer (51), there might be a risk that cancers were missed or underestimated in terms of their size or Gleason score (5). This limitation could also explain the high false-positive rate of SWE. Another limitation of using biopsy results as the reference standard is the lack of

Table 3

Pairwise AUC*st* Values according to Gleason Scores

Parameter	Benign	Gleason Score 6	Gleason Score 7	Gleason Score 8	Gleason Score 9
Benign	...	93 (89, 97)	86 (80, 92)	97 (95, 99)	99 (99, 100)
Gleason score 6	93 (89, 97)	...	46 (34, 58)	68 (48, 88)	98 (94, 100)
Gleason score 7	86 (80, 92)	46 (34, 58)	...	70 (54, 96)	96 (92, 100)
Gleason score 8	97 (95, 99)	68 (48, 88)	70 (54, 96)	...	83 (63, 100)
Gleason score 9	99 (99, 100)	98 (92, 100)	96 (92, 100)	83 (63, 100)	...

Note.—Data are AUC*st* values, as percentages, with 95% CIs in parentheses. In this study, there were five categories corresponding to the reference standard outcome (histologic Gleason scores): category 1 indicated benign tissue, and categories 2, 3, 4, and 5 indicated Gleason scores of 6, 7, 8, and 9, respectively.

Figure 7

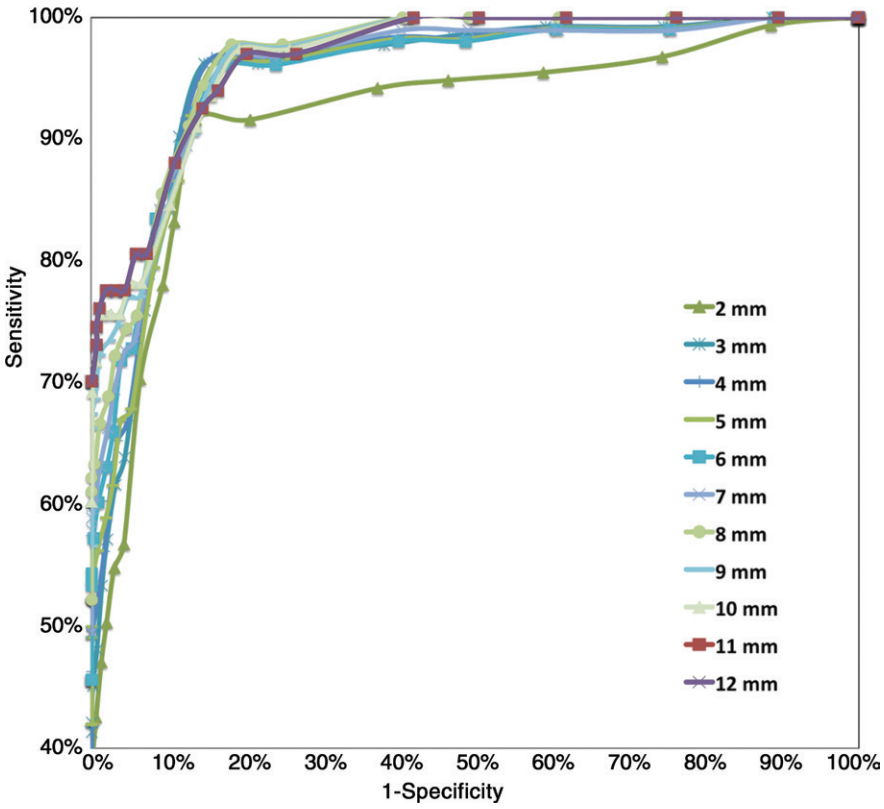

Figure 7: ROC curve for the performance of SWE as a function of minimal prostate cancer size for sizes ranging from 2 to 12 mm.

precise correlation between prostate cancer location and SWE estimates (ie, the stiff areas at SWE may not have been the actual cancer but tissues near a cancer).

Other limitations of this study included the lack of inter- and intraobserver variability data and analysis; the use of our data to establish thresholds, which can lead to overoptimistic results; and the limited number of cases of sextants with Gleason 8 and 9 scores.

Prostate SWE imaging is also facing some challenges. When a stiff area is detected during the examination, the operator should release any pressure on the transducer and image the lesion with different angles to avoid a misdiagnosis of prostate cancer. The posterior prostate parenchyma sitting just against the transducer appears stiff in some cases owing to the natural compression of the transducer resulting from bending the probe to image the prostate. Our study was limited to the detection and characterization of prostate cancer in the peripheral zone. Further studies need to be performed to assess transition zone prostate cancers. This study was also limited by a relatively small number of cases. Our cutoff values of 35 kPa for sextants and 38 kPa for patients need be validated in a larger multicentric clinical study. Macro- and microcalcifications may increase elasticity values. However, they can be easily identified with B-mode imaging. We did not consider eliminating the sextants that exhibited such findings, which may explain some highly elevated elasticity values despite the absence of prostate cancer.

In summary, SWE enables the assessment of tissue stiffness to provide additional information for the detection and biopsy guidance of prostate cancer. Indeed, SWE provides a high sensitivity for prostate cancer detection while also yielding a very high NPV, ensuring that only a very few cancers are or no cancer is missed in the prostate peripheral zone, even for Gleason 6 and small cancers (starting at 3 mm). Prostate cancer elasticity values increase with Gleason score and therefore seem linked to prostate cancer aggressiveness, especially for elevated Gleason scores (≥7).

Future studies should also involve three- or four-dimensional prostate SWE with multiplanar reconstruction and MR imaging fusion to volumetric US data that include elastographic data. These new modalities should improve guiding capabilities to target biopsies to the most suspicious areas.

Disclosures of Conflicts of Interest: J.M.C. Activities related to the present article: received an equipment loan from SuperSonic Imagine. Activities not related to the present article: is on the speakers bureaus of Bracco, Toshiba Medical Systems, SuperSonic Imagine, and Philips Healthcare; is a member of the advisory board of Philips Ultrasound. Other relationships: none to disclose. **A.M.T.** disclosed no relevant rela-

tionships. **A.K.** disclosed no relevant relationships. **V.V.** disclosed no relevant relationships. **A.M.** disclosed no relevant relationships. **O.H.** disclosed no relevant relationships. **R.M.** disclosed no relevant relationships. **R.G.B.** Activities related to the present article: received an equipment loan from SuperSonic Imagine. Activities not related to the present article: has received equipment grants from Philips Ultrasound, Siemens Ultrasound, and Esaote; is on the speakers bureaus of Philips Ultrasound, Siemens Ultrasound, and SuperSonic Imagine; is on the advisory panels of Philips Ultrasound, Siemens Ultrasound, and Toshiba America Medical Systems; has received a research grant from Bracco Diagnostic. Other relationships: none to disclose.

References

1. American Cancer Society. 2012 Estimates for Cancer Incidence. Atlanta, Ga: American Cancer Society, 2012.
2. Kelloff GJ, Choyke P, Coffey DS; Prostate Cancer Imaging Working Group. Challenges in clinical prostate cancer: role of imaging. AJR Am J Roentgenol 2009;192(6):1455–1470.
3. Singh H, Canto EI, Shariat SF, et al. Predictors of prostate cancer after initial negative systematic 12 core biopsy. J Urol 2004;171(5):1850–1854.
4. Mian BM, Naya Y, Okihara K, Vakar-Lopez F, Troncoso P, Babaian RJ. Predictors of cancer in repeat extended multisite prostate biopsy in men with previous negative extended multisite biopsy. Urology 2002;60(5):836–840.
5. Taira AV, Merrick GS, Galbreath RW, et al. Performance of transperineal template-guided mapping biopsy in detecting prostate cancer in the initial and repeat biopsy setting. Prostate Cancer Prostatic Dis 2010;13(1):71–77.
6. Djavan B, Remzi M, Marberger M. When to biopsy and when to stop biopsying. Urol Clin North Am 2003;30(2):253–262, viii.
7. Delongchamps NB, Haas GP. Saturation biopsies for prostate cancer: current uses and future prospects. Nat Rev Urol 2009;6(12):645–652.
8. Giannarini G, Autorino R, di Lorenzo G. Saturation biopsy of the prostate: why saturation does not saturate. Eur Urol 2009;56(4):619–621.
9. Ashley RA, Inman BA, Routh JC, Mynderse LA, Gettman MT, Blute ML. Reassessing the diagnostic yield of saturation biopsy of the prostate. Eur Urol 2008;53(5):976–981.
10. Pepe P, Fraggetta F, Galia A, Grasso G, Aragona F. Prostate cancer detection by TURP after repeated negative saturation biopsy in patients with persistent suspicion of cancer: a case-control study on 75 consecutive patients. Prostate Cancer Prostatic Dis 2010;13(1):83–86.
11. Girouin N, Mège-Lechevallier F, Tonina Senes A, et al. Prostate dynamic contrast-enhanced MRI with simple visual diagnostic criteria: is it reasonable? Eur Radiol 2007;17(6):1498–1509.
12. Villers A, Puech P, Mouton D, Leroy X, Ballereau C, Lemaitre L. Dynamic contrast enhanced, pelvic phased array magnetic resonance imaging of localized prostate cancer for predicting tumor volume: correlation with radical prostatectomy findings. J Urol 2006;176(6 Pt 1):2432–2437.
13. Fütterer JJ, Heijmink SW, Scheenen TW, et al. Prostate cancer localization with dynamic contrast-enhanced MR imaging and proton MR spectroscopic imaging. Radiology 2006;241(2):449–458.
14. Lemaitre L, Puech P, Poncelet E, et al. Dynamic contrast-enhanced MRI of anterior prostate cancer: morphometric assessment and correlation with radical prostatectomy findings. Eur Radiol 2009;19(2):470–480.
15. Lim HK, Kim JK, Kim KA, Cho KS. Prostate cancer: apparent diffusion coefficient map with T2-weighted images for detection—a multireader study. Radiology 2009;250(1):145–151.
16. Jung AJ, Westphalen AC. Imaging prostate cancer. Radiol Clin North Am 2012;50(6):1043–1059.
17. Tanimoto A, Nakashima J, Kohno H, Shinmoto H, Kuribayashi S. Prostate cancer screening: the clinical value of diffusion-weighted imaging and dynamic MR imaging in combination with T2-weighted imaging. J Magn Reson Imaging 2007;25(1):146–152.
18. Yoshizako T, Wada A, Hayashi T, et al. Usefulness of diffusion-weighted imaging and dynamic contrast-enhanced magnetic resonance imaging in the diagnosis of prostate transition-zone cancer. Acta Radiol 2008;49(10):1207–1213.
19. Cheikh AB, Girouin N, Colombel M, et al. Evaluation of T2-weighted and dynamic contrast-enhanced MRI in localizing prostate cancer before repeat biopsy. Eur Radiol 2009;19(3):770–778.
20. Ocak I, Bernardo M, Metzger G, et al. Dynamic contrast-enhanced MRI of prostate cancer at 3 T: a study of pharmacokinetic parameters. AJR Am J Roentgenol 2007;189(4):849.
21. Vargas HA, Akin O, Afaq A, et al. Magnetic resonance imaging for predicting prostate biopsy findings in patients considered for active surveillance of clinically low risk prostate cancer. J Urol 2012;188(5):1732–1738.
22. Dickinson L, Ahmed HU, Allen C, et al. Magnetic resonance imaging for the detection, localisation, and characterisation of prostate cancer: recommendations from a European consensus meeting. Eur Urol 2011;59(4):477–494.
23. Langer DL, van der Kwast TH, Evans AJ, Trachtenberg J, Wilson BC, Haider MA. Prostate cancer detection with multi-parametric MRI: logistic regression analysis of quantitative T2, diffusion-weighted imaging, and dynamic contrast-enhanced MRI. J Magn Reson Imaging 2009;30(2):327–334.
24. Vargas HA, Akin O, Shukla-Dave A, et al. Performance characteristics of MR imaging in the evaluation of clinically low-risk prostate cancer: a prospective study. Radiology 2012;265(2):478–487.
25. Pinto F, Totaro A, Calarco A, et al. Imaging in prostate cancer diagnosis: present role and future perspectives. Urol Int 2011;86(4):373–382.
26. Norberg M, Egevad L, Holmberg L, Sparén P, Norlén BJ, Busch C. The sextant protocol for ultrasound-guided core biopsies of the prostate underestimates the presence of cancer. Urology 1997;50(4):562–566.
27. Rifkin MD, Zerhouni EA, Gatsonis CA, et al. Comparison of magnetic resonance imaging and ultrasonography in staging early prostate cancer: results of a multi-institutional cooperative trial. N Engl J Med 1990;323(10):621–626.
28. Beerlage HP, Aarnink RG, Ruijter ET, et al. Correlation of transrectal ultrasound, computer analysis of transrectal ultrasound and histopathology of radical prostatectomy specimen. Prostate Cancer Prostatic Dis 2001;4(1):56–62.
29. Wijkstra H, Wink MH, de la Rosette JJ. Contrast specific imaging in the detection and localization of prostate cancer. World J Urol 2004;22(5):346–350.
30. Aigner F, Pallwein L, Mitterberger M, et al. Contrast-enhanced ultrasonography using cadence-contrast pulse sequencing technology for targeted biopsy of the prostate. BJU Int 2009;103(4):458–463.
31. Hoyt K, Castaneda B, Zhang M, et al. Tissue elasticity properties as biomarkers for prostate cancer. Cancer Biomark 2008;4(4-5):213–225.

32. Pallwein L, Mitterberger M, Struve P, et al. Real-time elastography for detecting prostate cancer: preliminary experience. BJU Int 2007;100(1):42–46.

33. Salomon G, Köllerman J, Thederan I, et al. Evaluation of prostate cancer detection with ultrasound real-time elastography: a comparison with step section pathological analysis after radical prostatectomy. Eur Urol 2008;54(6):1354–1362.

34. Walz J, Marcy M, Pianna JT, et al. Identification of the prostate cancer index lesion by real-time elastography: considerations for focal therapy of prostate cancer. World J Urol 2011;29(5):589–594.

35. Brock M, von Bodman C, Palisaar RJ, et al. The impact of real-time elastography guiding a systematic prostate biopsy to improve cancer detection rate: a prospective study of 353 patients. J Urol 2012;187(6):2039–2043.

36. Tsutsumi M, Miyagawa T, Matsumura T, et al. The impact of real-time tissue elasticity imaging (elastography) on the detection of prostate cancer: clinicopathological analysis. Int J Clin Oncol 2007;12(4):250–255.

37. Zhai L, Polascik TJ, Foo WC, et al. Acoustic radiation force impulse imaging of human prostates: initial in vivo demonstration. Ultrasound Med Biol 2012;38(1):50–61.

38. Sahebjavaher RS, Frew S, Bylinskii A, et al. Prostate MR elastography with transperineal electromagnetic actuation and a fast fractionally encoded steady-state gradient echo sequence. NMR Biomed 2014;27(7):784–794.

39. Thörmer G, Reiss-Zimmermann M, Otto J, et al. Novel technique for MR elastography of the prostate using a modified standard endorectal coil as actuator. J Magn Reson Imaging 2013;37(6):1480–1485.

40. Bercoff J, Tanter M, Fink M. Supersonic shear imaging: a new technique for soft tissue elasticity mapping. IEEE Trans Ultrason Ferroelectr Freq Control 2004;51(4):396–409.

41. Fink M, Tanter M. Multiwave imaging and super resolution. Phys Today 2010;63(2):28–33.

42. Barr RG, Memo R, Schaub CR. Shear wave ultrasound elastography of the prostate: initial results. Ultrasound Q 2012;28(1):13–20.

43. Correas JM, Khairoune A, Tissier AM, Vasiliu V, Méjean A, Hélénon O. Trans-rectal quantitative shear wave elastography: application to prostate cancer a feasibility study. Presented at the 24th European Congress of Radiology, Vienna, Austria, 2012.

44. Ahmad S, Cao R, Varghese T, Bidaut L, Nabi G. Transrectal quantitative shear wave elastography in the detection and characterisation of prostate cancer. Surg Endosc 2013;27(9):3280–3287.

45. Heidenreich A, Bastian PJ, Bellmunt J, et al. EAU guidelines on prostate cancer. I. Screening, diagnosis, and local treatment with curative intent-update 2013. Eur Urol 2014;65(1):124–137.

46. Russo AL, Chen MH, Aizer AA, Hattangadi JA, D'Amico AV. Advancing age within established Gleason score categories and the risk of prostate cancer-specific mortality (PCSM). BJU Int 2012;110(7):973–979.

47. Obuchowski NA. Nonparametric analysis of clustered ROC curve data. Biometrics 1997;53(2):567–578.

48. Obuchowski NA, Lieber ML, Powell KA. Data analysis for detection and localization of multiple abnormalities with application to mammography. Acad Radiol 2000;7(7):516–525.

49. Obuchowski NA. Estimating and comparing diagnostic tests' accuracy when the gold standard is not binary. Acad Radiol 2005;12(9):1198–1204.

50. Barr RG. Real-time ultrasound elasticity of the breast: initial clinical results. Ultrasound Q 2010;26(2):61–66.

51. Smith RA, Cokkinides V, Eyre HJ. Cancer screening in the United States, 2007: a review of current guidelines, practices, and prospects. CA Cancer J Clin 2007;57(2):90–104.